

REPORT DOCUMENTATION PAGE			Form Approved OMB No. 074-0188	
Public reporting burden for this collection of information is estimated to average 1 hour per response, including the time for reviewing instructions, searching existing data sources, gathering and maintaining the data needed, and completing and reviewing this collection of information. Send comments regarding this burden estimate or any other aspect of this collection of information, including suggestions for reducing this burden to Washington Headquarters Services, Directorate for Information Operations and Reports, 1215 Jefferson Davis Highway, Suite 1204, Arlington, VA 22202-4302, and to the Office of Management and Budget, Paperwork Reduction Project (0704-0188), Washington, DC 20503				
1. AGENCY USE ONLY (Leave blank)	2. REPORT DATE 06/31/2013	3. REPORT TYPE AND DATES COVERED Final Performance Report, 04/14/10-04/13/13		
4. TITLE AND SUBTITLE INTEGRATED STUDY OF FLIGHT STABILIZATION WITH FLAPPING WINGS IN CANONICAL URBAN FLOWS		5. FUNDING NUMBERS FA9550-10-1-0062		
6. AUTHOR(S) Rajat Mittal, PhD Tyson Hedrick, PhD				
7. PERFORMING ORGANIZATION NAME(S) AND ADDRESS(ES) Johns Hopkins University 3400 N. Charles St. Baltimore, MD 21218 University of North Carolina at Chapel-Hill; Chapel Hill, NC 27599		8. PERFORMING ORGANIZATION REPORT NUMBER		
9. SPONSORING / MONITORING AGENCY NAME(S) AND ADDRESS(ES) AFOSR 4015 Wilson Boulevard Room 713 Arlington VA 22203-1954		10. SPONSORING / MONITORING AGENCY REPORT NUMBER		
11. SUPPLEMENTARY NOTES				
12a. DISTRIBUTION / AVAILABILITY STATEMENT Approved for public release; distribution unlimited.			12b. DISTRIBUTION CODE	
13. ABSTRACT (Maximum 200 Words) An integrated numerical-experimental methodology is used to investigate the aerodynamics and coupled flight dynamics of insects in free flight. The experimental component, which involves quantitative, high-speed videogrammetry of insects in free flight along with measurements of the mass properties of the insect body and wings, provides data for the parameterization as well as the validation of the computational models. The computational component of the research is centered primarily on high-fidelity Navier-Stokes (NS) modeling, which is based on a sharp interface immersed boundary method. The first part of the study involves the development and validation of a high-fidelity Navier-Stokes model of a hovering hawkmoth. The simulations are used for a comparative study of the hovering efficiency of flapping and revolving wings. The second phase of the study focuses on the stability of insect and insect-inspired flight. Stability analysis as well as fully coupled aero-flight dynamics modeling is used to gain insights into the stability properties of hovering insects. Combining this with experimental observations leads to a bioinspired strategy for flight stabilization, which is then tested via the computational modeling approach.				
14. SUBJECT TERMS Flapping Flight, Micro-Aerial Vehicles, Unsteady Aerodynamics, Flight Dynamics, Urban Flows			15. NUMBER OF PAGES 10	
			16. PRICE CODE	
17. SECURITY CLASSIFICATION OF REPORT Unclassified	18. SECURITY CLASSIFICATION OF THIS PAGE Unclassified	19. SECURITY CLASSIFICATION OF ABSTRACT Unclassified	20. LIMITATION OF ABSTRACT UU	

NSN 7540-01-280-5500

Standard Form 298 (Rev. 2-89)
Prescribed by ANSI Std. Z39-18
298-102

INTEGRATED STUDY OF FLIGHT STABILIZATION WITH FLAPPING WINGS IN CANONICAL URBAN FLOWS

Rajat Mittal (Johns Hopkins University)

Tyson Hedrick (University of North-Carolina at Chapel Hill)

I. Objectives

The objective of the proposed project was to understand how animals stabilize their flight in unsteady flows that are representative of urban environments. These environments pose unique challenges for flapping wing micro-aerial vehicles (MAVs) (see **Fig. 1**). While operating below rooftop level, MAVs will encounter highly unsteady flows associated with building wakes, regions of high flow velocity created in narrow passages, shear layers, as well as energetic recirculating corner flows. Successful operation will

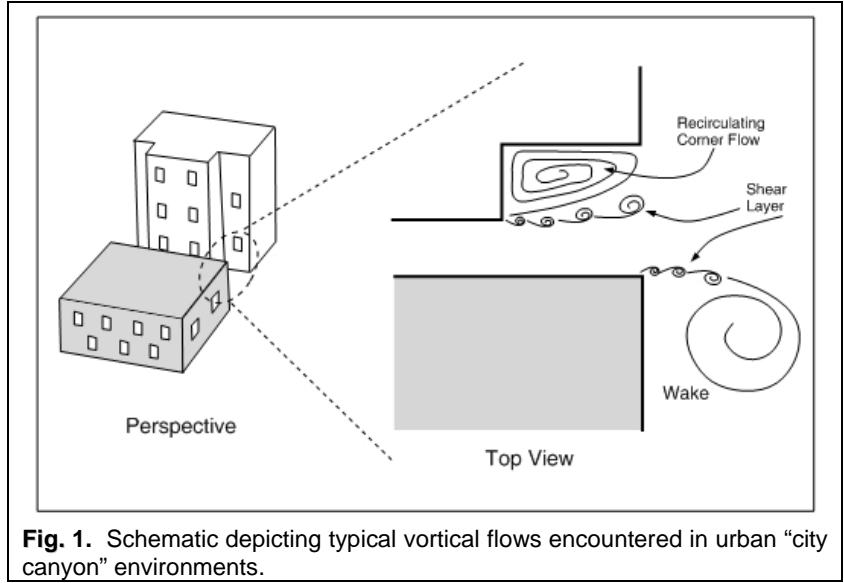


Fig. 1. Schematic depicting typical vortical flows encountered in urban “city canyon” environments.

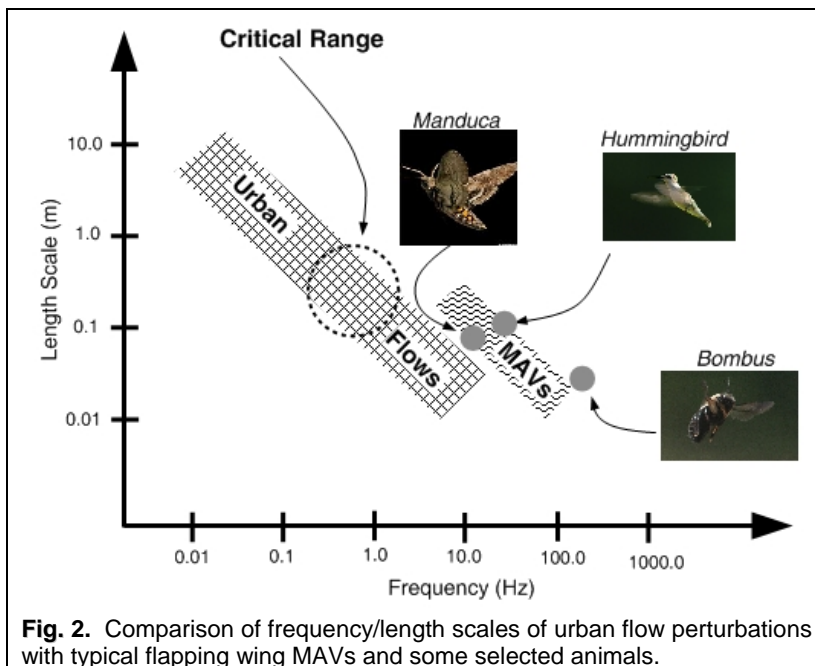
therefore require that MAVs be able to stabilize their flight in such an environment. The primary focus of the project was to gain insights into how animals modify wing kinematics and exploit wing, as well as body deformation when flying in a perturbed environment. The computational modeling employed a high-fidelity CFD-FSI tool that is based on a Navier-Stokes immersed-boundary solver. This 3-D, parallelized, DNS/LES solver simulates flows with complex moving boundaries on stationary Cartesian grids, and is well suited for this research. The experiments employed high-speed, high resolution videogrammetry of hawkmoths and butterflies in free flight. Controlled aerodynamic perturbations were provided in ways designed to elicit specific dynamical responses. In addition to the aerodynamic forces and mechanisms, we studied how insects manipulate their inertial properties during complex flight regimes. The study employed un-tethered insect flight experiments coupled with computational modeling of the aerodynamics. Sophisticated flight dynamics models were developed based on the experimental/computational analysis, and used to explore new concepts for stabilizing and controlling bioinspired, flapping wing MAVs.

II. Background

To better understand the challenge for MAVs in urban flows, consider the flow associated with a building that has a characteristic size of 10 meters, and a nominal wind speed of 2 m/s. Given a universal Strouhal number of about 0.16 (Roshko 1954), the Kármán vortex shedding from such a building would occur at a frequency (f_K) of about 0.03 Hz. While this frequency is significantly lower than the typical wing flapping frequency of a MAV (which would be in the 10-100 Hz range), the frequency of vortex rollup in the separated shear layer, which scales as $f_{SL} \sim 0.02 \text{Re}^{0.67} f_K$ (Prasad and Williamson 1996), would be about 10 Hz. While f_K and f_{SL} represent lower and upper bounds of the energetic range, non-linear interactions in the flow will, in fact, produce energetic scales at all intermediate frequencies. The length scales of these perturbations will also range from $O(10\text{m})$ (for the wake) down to a few centimeters for the smallest shear layer eddies. This is schematically shown in **Fig. 2**. Furthermore, given that typical

perturbation velocities in a shear layer can be as high as 50% of the freestream velocity (Balachandar et al. 1997), MAVs in an urban environment could experience velocity perturbations of about a meter per second or more.

Of all the aerodynamic perturbations, those with time and length scales which are one to two orders of magnitude larger than the MAV (denoted as the “critical range” in Fig. 2) are expected to be most troublesome. On the one hand, these scales are small/rapid enough that they cannot be considered to be in the “quasi-steady” regime for MAVs, and on the other, they are large enough to produce significant perturbation magnitudes. The simple scaling analysis described above clearly shows that such perturbations are indeed expected to be present in urban flows, and therefore, MAVs will have to be designed to operate (fly, hover, and perhaps, perch and take-off) in the presence of such perturbed flows. Furthermore, negotiating tight exterior as well as interior (inside buildings) flight paths requires a high level of maneuverability. At the same time, MAVs have to be able to stabilize their flight in unsteady environments when required, and also be robust enough to remain operational despite incidental contact with solid objects. These are some of the key challenges for MAV design. It should be noted that atmospheric turbulence also poses somewhat similar challenges for flapping wings MAVs and although the current proposal was targeted specifically at urban environments, much of what has been learnt here is also relevant to MAV flight in atmospheric turbulence.



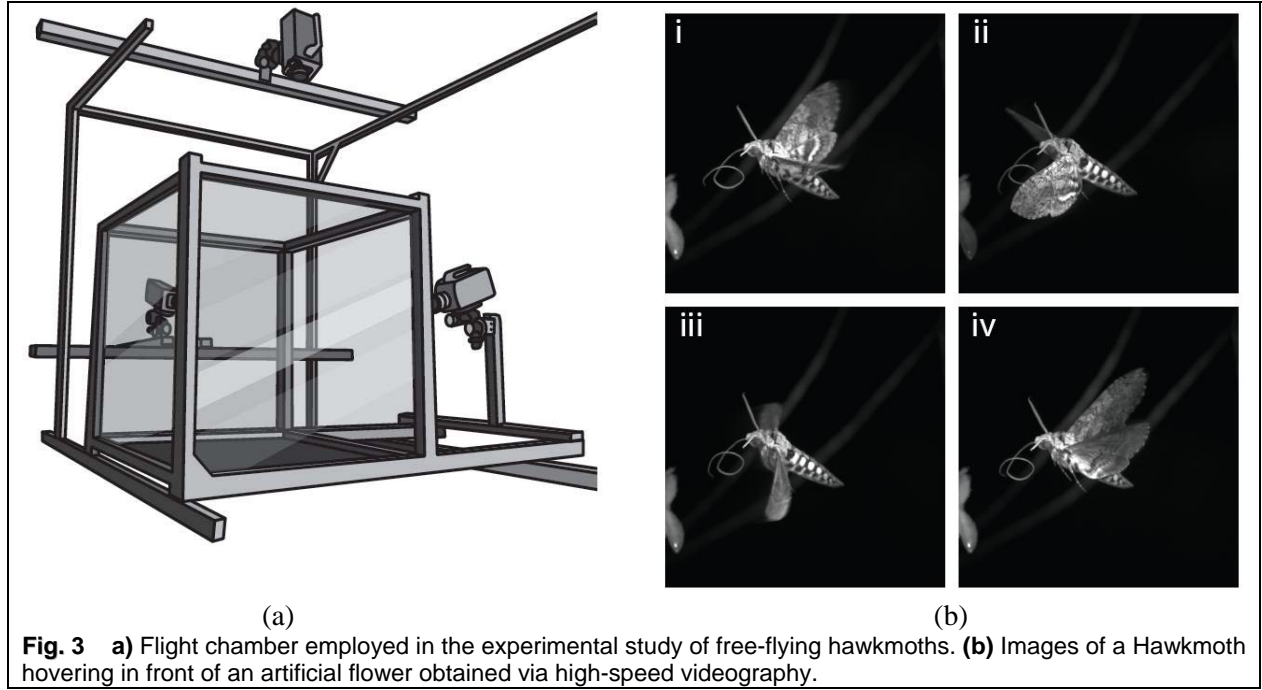
III. Status of Effort

The effort has been successful in accomplishing all of its original objectives. In Section IV below we provide a detailed description of the major accomplishment and new findings.

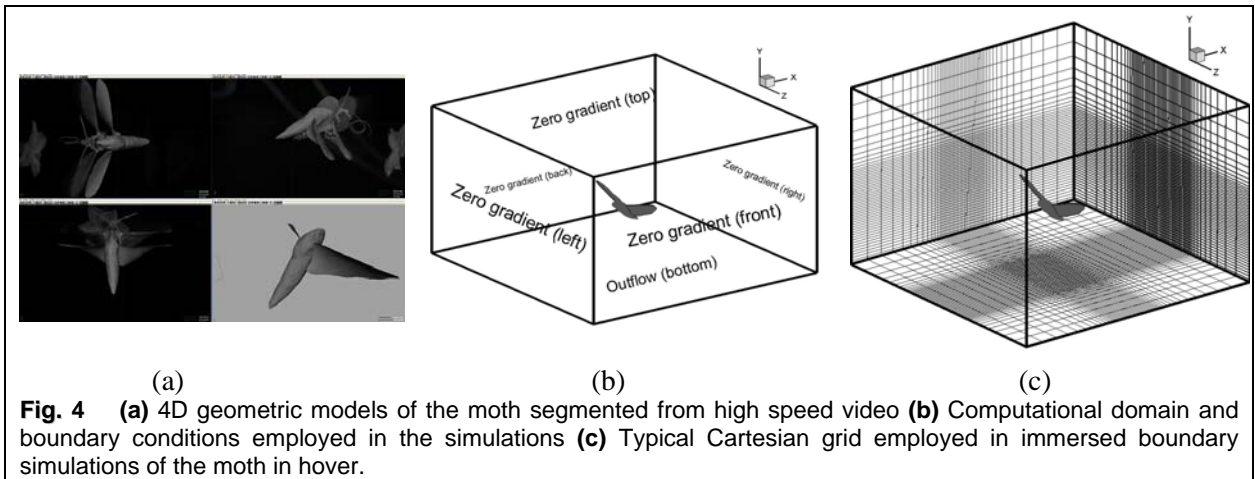
IV. Accomplishments and New Findings

A. Computational Modeling of Insect Inspired Flapping Wing Flows

A critical first step in CFD based analysis of flight stability of insects is to demonstrate the ability of CFD to accurately predict all the quantities of interest (such as time-varying lift, drag and moments). This was accomplished by performing a comprehensive validation study for a hovering Hawkmoth. The hawkmoth species examined here, *Manduca sexta*, is a relatively large (~2g body mass, 10cm wing span), nectivorous insect with a number of characteristics that make it and its close relatives particularly useful subjects in laboratory studies of animal flight. The moths were recorded while hovering in front of an artificial flower in a glass-walled flight chamber by a set of three orthogonally positioned high-speed video cameras (see Fig. 3). Three-dimensional kinematics were obtained by tracking the location of the left and right wing base, wing tip, and the forewing notch on the trailing edge of the wing, the center of the head, the thorax-abdomen junction and the tip of the abdomen through 4.5 successive hovering wingbeats including the wingbeat used for the Navier-Stokes analysis (see Fig. 4a). Next, the 3D location



of the center-of-mass for each of the four body segments (left wing, right wing, thorax (including head) and abdomen) was estimated. We then computed the segment accelerations by taking the second-derivative with respect to time and adding a gravitational acceleration of 9.81 ms^{-2} . These 3D accelerations were then converted to forces by multiplying by the segment masses and added together to reveal the net instantaneous aerodynamic force exerted on the moth.



A sharp-interface immersed-boundary method (Mittal & Iaccarino 2005) described in Mittal et al. (2008) and Seo et al. (2011) has been used in these simulations. The governing equations are the three-dimensional unsteady, viscous incompressible Navier-Stokes equations. The effect of the immersed boundary on the flow is incorporated by using a multi-dimensional ghost-cell methodology. This method falls in the category of sharp-interface discrete forcing immersed boundary methods (Mittal & Iaccarino 2005). The current method employs an unstructured grid with triangular elements to represent the surface of three-dimensional bodies such as the insect wings, which is immersed into the Cartesian volume grid (**Fig. 4**). The ghost-cells are defined as the cells inside the solid that have at least one neighbor in the fluid. The second-order accurate discretization on the body surface along with the second-order accuracy

of the fluid cells leads to second-order local and global spatial accuracy in the computations (Mittal et al. 2008).

Figure 5 panels (a) to (d) show the vortex structures around the body and wings of the hovering moth during one cycle. A distinct leading-edge vortex (LEV) is generated at the beginning of downstroke. In addition, a tip-vortex (TE) and a trailing-edge vortex (TEV) are also generated from each wing and these are observed to wrap around the wing. Later, as the wings start to accelerate downwards (**Fig. 5b**) the LEVs and TEVs grow in size and the TEVs are shed from the wings. The LEV covers a large part of the wing surface and accounts for the lift peak during downstroke; **Fig. 5(e)** show an isosurface of negative (suction) pressure at $t/T = 0.25$ and this clearly shows the large region of suction pressure on the top surface of the wing due to the strong LEV. During upstroke (**Fig. 5c & 5d**), the LEVs are much weaker than those during downstroke due to a reduced effective angle-of-attack of the leading-edge and the corresponding suction pressure in **Fig. 5f** is significantly diminished.

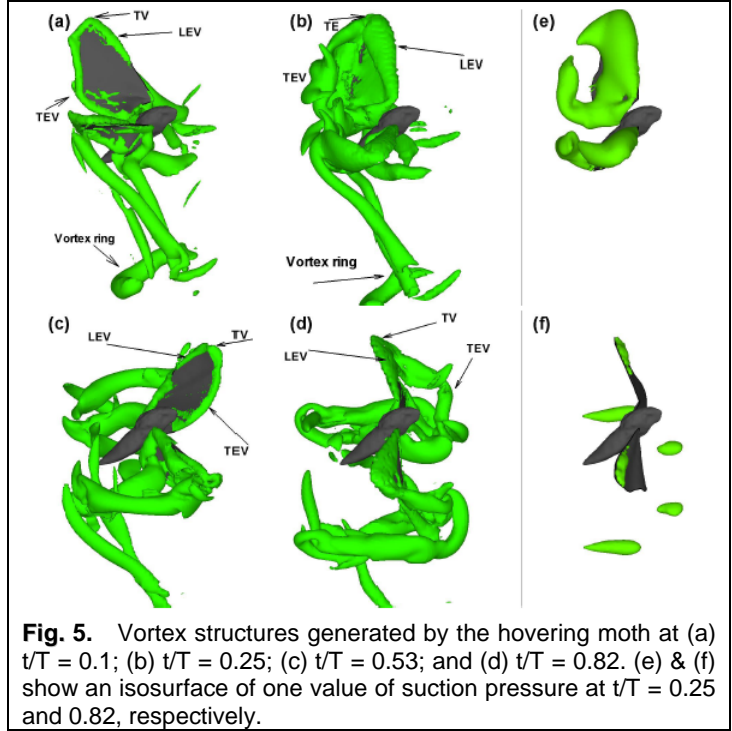


Fig. 5. Vortex structures generated by the hovering moth at (a) $t/T = 0.1$; (b) $t/T = 0.25$; (c) $t/T = 0.53$; and (d) $t/T = 0.82$. (e) & (f) show an isosurface of one value of suction pressure at $t/T = 0.25$ and 0.82 , respectively.

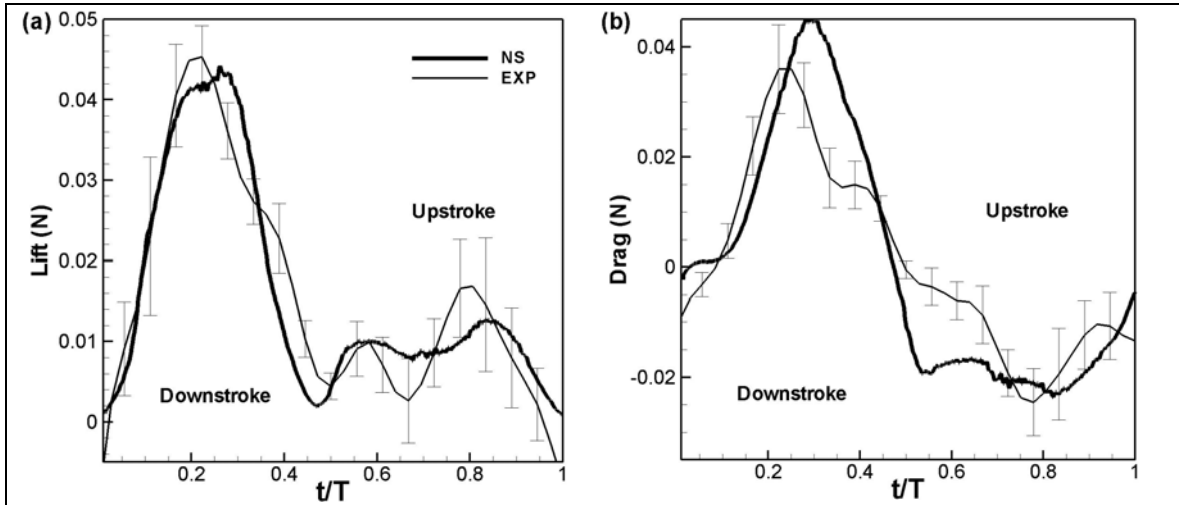


Fig. 6. A comparison of the instantaneous vertical (a) and horizontal (b) force between the Navier-Stokes CFD model and the experimental results.

Figure 6 shows a comparison of the time-varying vertical and horizontal forces obtained from the experiments as well as Navier-Stokes simulation. The NS simulation was based on a cyclical repetition of the one recorded flapping stroke. First, for the NS simulation, the average lift produced by the two wings is 14.9 mN and this matches reasonably well with the weight of the insect (13.6 mN). In addition, **Fig. 6(a)** indicates that the time variation of the vertical force in the NS simulation also agrees quite well with the experimental result. The NS simulation very accurately predicts the rise of the lift force during the initial phase of the downstroke as well as the peak lift value of about 44 mN. The agreement between the two during the latter half of the downstroke is also quite good with the simulated value falling mostly within the variability of the experiments. The upstroke is found to produce lower values of lift but the

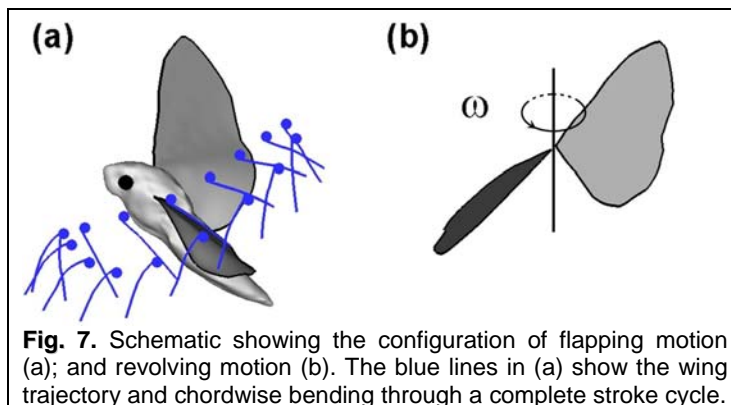
experimental variability is of the same magnitude as for the downstroke. In terms of the comparison, the NS simulation correctly indicates the presence of two small peaks in lift during the upstroke but tends to over-predict the lift at mid-upstroke. At all other phases during the upstroke, the computed values lie within the experimental variability. The mean value of the computed lift, which is 14.9 mN, matches very well with the mean experimental value of 15.0 mN.

The match is less precise for the horizontal forces (**Fig. 6b**), but the simulation does predict the key features of the overall time-course reasonably well. First, the wings produce a drag force during downstroke and a thrust force during upstroke. The drag and thrust nearly cancel each other during one flapping cycle for the hawkmoth in hover in both the simulation and the experiment. The horizontal force peak during downstroke is sharper and larger than that during upstroke. This trend which is due to the strong leading-edge vortex formed in downstroke is also captured correctly in the simulation. The peak value of drag force during downstroke in the experiment is 35 ± 8 mN from the experiment, whereas CFD predicts a value of 45 mN. The matches in the RMS values of drag are also reasonable with the computations predicting a cycle-averaged RMS of 20.9mN and the experiments, a value of 17.0mN. It should be noted that while some past modeling studies have found a reasonable match between the computed mean lift value and the weight of the insect (Aono et al. 2008), no past study has successfully validated the computed time-varying lift and drag with a corresponding experiment.

The simulations also allow us to estimate the power expended in producing the lift force and this is done by integrating the pressure and shear associated work on the surface of the wing. This quantity is an essential component of hovering efficiency but is not obtainable directly from insect flight experiments. Note that power is obtained from a dot-product between the local time-varying aerodynamic force and wing velocity. Since we have matched the local wing velocity closely with experimental data and also demonstrated a reasonably accurate prediction of the time-varying forces on the wing, we can be reasonably assured that the aerodynamic power estimated from our computations is fairly accurate; we found that the moth uses about 66mW of power per cycle during hover. Following Stevenson et al. (1990), we estimate that 21% of the hawkmoth's mass is flight muscle, giving a muscle mass-specific power of approximately 230 Wkg^{-1} . This result is consistent with the measured oxygen consumption of hovering *Manduca* of $12.2 \text{ ml O}_2 \text{ min}^{-1}$, which at 20% muscle efficiency and 20% flight muscle mass fraction also implies a power output of 230 Wkg^{-1} (Casey et al. 1976). Further results of this study can be found in Zheng et al. (2013b).

B. Comparative Study of Flight Efficiency of Flapping and Revolving Wings for MAV Applications

The power requirements for hovering flight in the hawkmoth revealed by the detailed Navier-Stokes simulation described above in Section A led us to examine the relative efficiency of bio-inspired flapping MAVs in comparison to rotating wing designs of the same wing and body scale. We used direct numerical simulations to explore the hovering performance and efficiency for hawkmoth-inspired flapping and revolving wings (**Fig. 7**) at Reynolds numbers varying from 50 to 4800. This range covers the gamut from small (fruit fly size) to large (hawkmoth size) flying insects and is also relevant to the design of micro- and nano-aerial vehicles. The flapping wing configuration used here corresponds to a hovering hawkmoth and the model is derived from high-speed videogrammetry of this insect as described in Section A. The revolving wing configuration also employs the wings of the hawkmoth but these are arranged in a dual-blade configuration typical of helicopters. Flow for both of these configurations is simulated over the range of Reynolds numbers of interest and the aerodynamic performance of the two compared. The comparison of these two seemingly different configurations raised issues regarding the



appropriateness of various performance metrics and even characteristic scales; these were also addressed in the current study. Finally, the difference in the performance between the two was correlated with the flow physics of the two configurations.

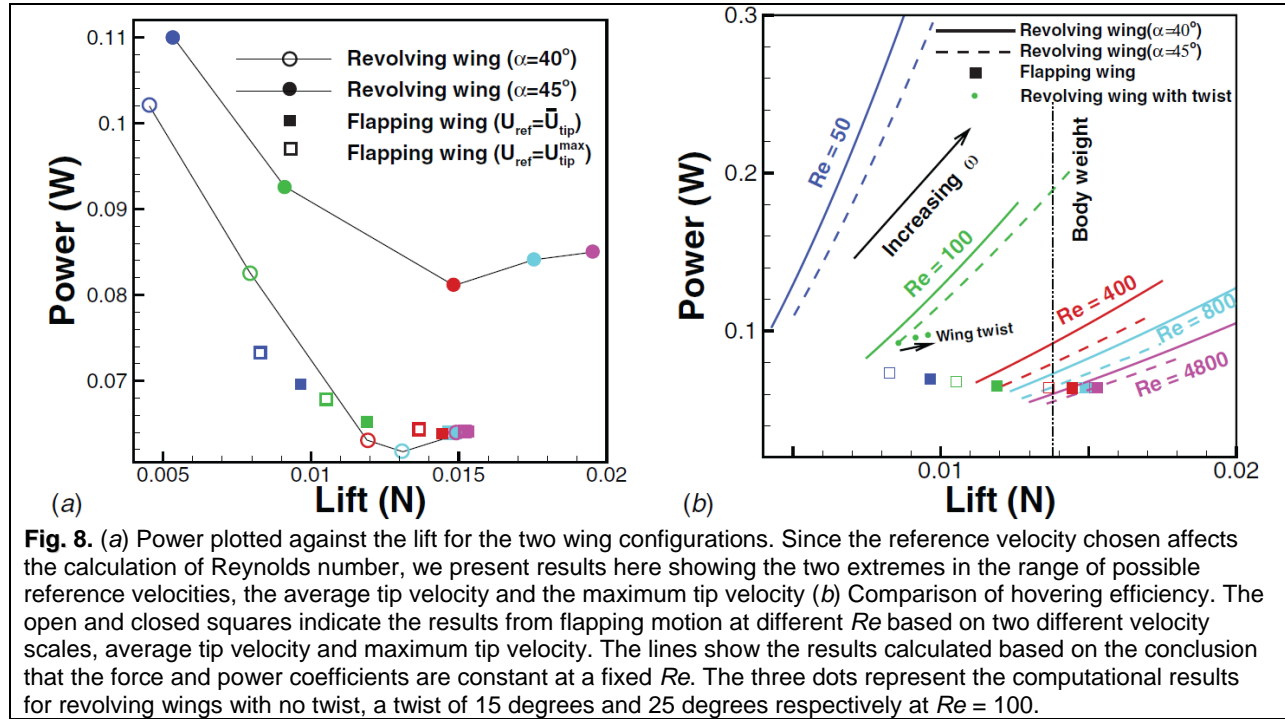


Fig. 8. (a) Power plotted against the lift for the two wing configurations. Since the reference velocity chosen affects the calculation of Reynolds number, we present results here showing the two extremes in the range of possible reference velocities, the average tip velocity and the maximum tip velocity (b) Comparison of hovering efficiency. The open and closed squares indicate the results from flapping motion at different Re based on two different velocity scales, average tip velocity and maximum tip velocity. The lines show the results calculated based on the conclusion that the force and power coefficients are constant at a fixed Re . The three dots represent the computational results for revolving wings with no twist, a twist of 15 degrees and 25 degrees respectively at $Re = 100$.

We found that the lift and the associated aerodynamic power provide the most objective metric for comparing the relative performance of these two configurations because variation in the wing velocity during the flapping cycle makes any particular choice of a reference velocity for non-dimensionalization arbitrary and uninformative. The simulations show that at a Reynolds number of about 5000, the revolving wing matches the lift production and power expenditure of the flapping wing. However, as the Reynolds number decreases, the performance of the revolving wing starts to lag that of the flapping wing. At a Reynolds number of about 100, the revolving wing requires at least a factor of 2 more power to produce a lift equivalent to the flapping wing (Fig. 8).

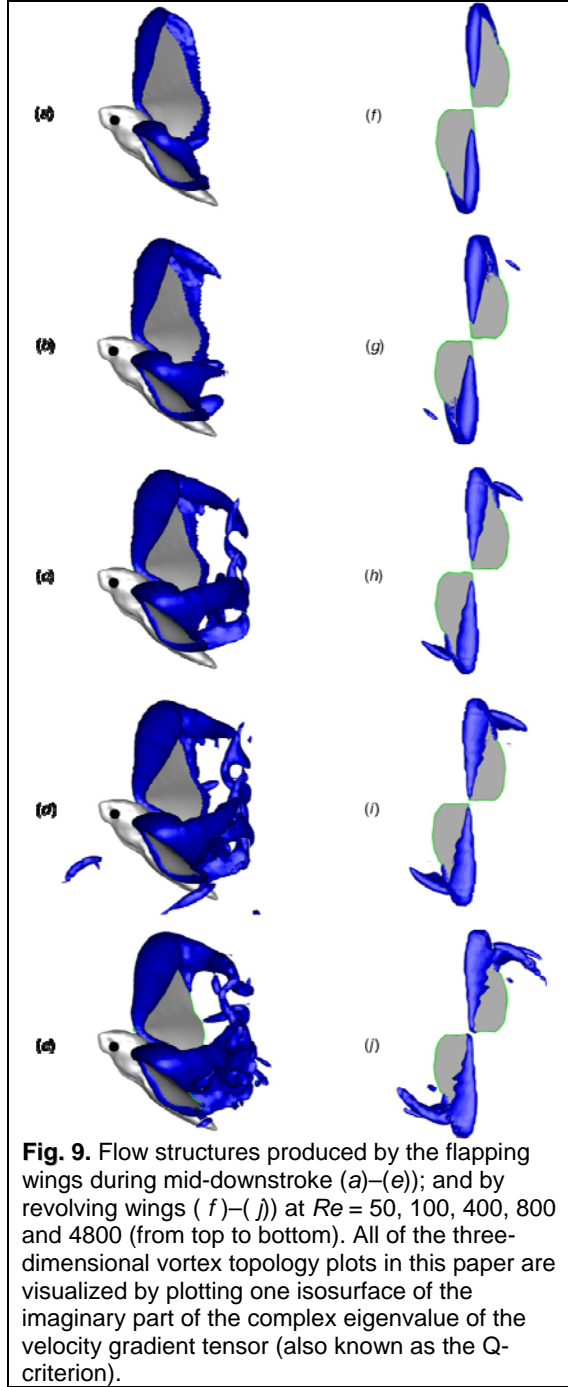
We examined various possible explanations for the different scaling of power with Reynolds number among the revolving and flapping wings. Explanations considered included: wing twist since the flapping wing included some twist while the revolving wing did not, wing-wing interaction, unsteady aerodynamic effects and viscous versus inviscid aerodynamic effects. The addition of wing-twist to the revolving wing model (Fig. 8b) led to incremental improvements in the lift to power ratio but was not sufficient to explain the differences in scaling between revolving and flapping wings.

Wing-wing interactions were considered by comparing revolving and flapping simulations with only 1 wing to simulations with 2 wings present (Table 1).

These revealed that revolving wings experience much greater wing-wing interactions than flapping wings, but the interactions do not affect the power loading, implying that the reductions in lift and power in the revolving two-wing case are due to downwash reducing the effective angle of attack. Thus, wing-wing interactions are also not a good explanation for differences between revolving and flapping wing power requirements.

	Lift (mN)	Power (mW)	Power loading (N/W)
Flapping (two wings)	14.9	64.0	0.23
Flapping (one wing) x2	14.6	59.9	0.24
Revolving (two wings)	17.5	84.1	0.21
Revolving (one wing) x2	20.6	96.1	0.21

Table 1: Comparison of lift, power and power loading for flapping and revolving motion (45 degree angle of attack) with one wing and two wings.



specimens that form the basis of this study. The obvious question that this raises is what the current study can say regarding the comparative performance of the two configurations at Reynolds numbers higher than 5000. Accurate computational modeling becomes increasingly challenging at higher Reynolds numbers since the grid requirements typically increase rapidly with this parameter. Experiments, therefore, remain the best way of accessing these higher Reynolds numbers. We note however that all the performance metrics (lift, power and power loading) in the current study show an asymptotic behavior as the higher Reynolds number is approached. Interestingly, experiments on revolving wings indicate that the vortex dynamics do not change significantly as the Reynolds number is increased from 10000 to 60000, which would support our observation. All of this suggests that barring the appearance of some additional flow mechanism(s), the overall trend at the Reynolds number of 4800 where the two

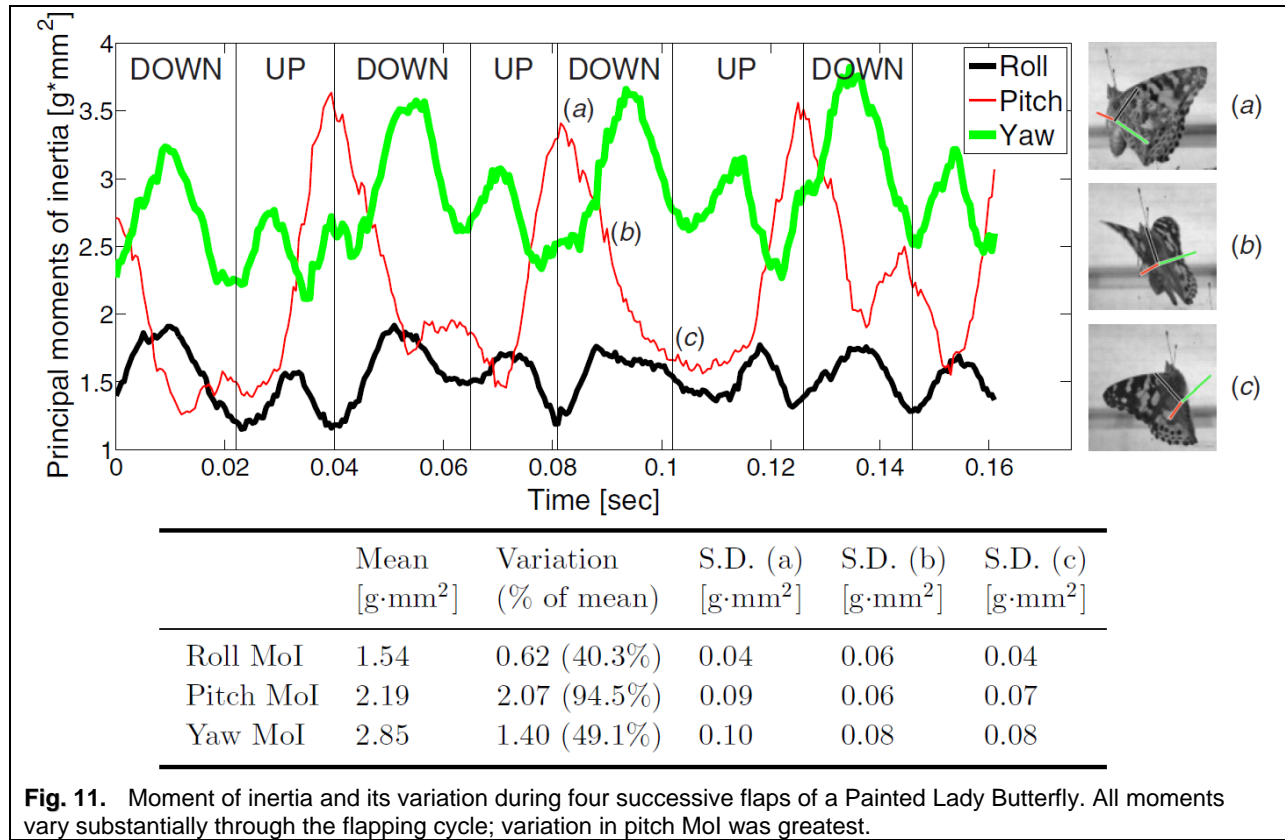
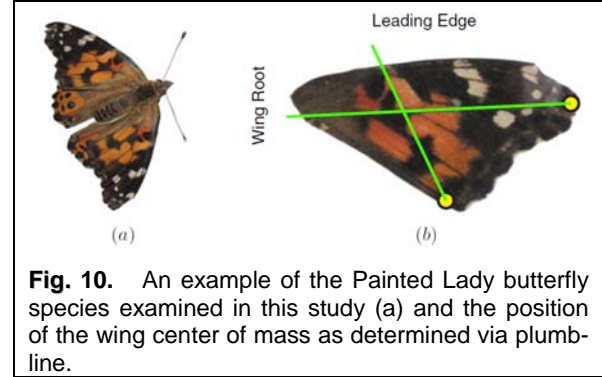
Unsteady aerodynamic effects in the form of a leading edge vortex (LEV) are well known source of unsteady aerodynamic lift in flapping wings (Ellington et al., 1996) and are also known to occur in rotating wings operating at a high angle of attack (e.g. Liu and Kawachi, 2001). Examination of the flow structures in the revolving and flapping wing simulations revealed the anticipated LEVs (**Fig. 9**), and it is clear that during mid-downstroke, the LEV of the flapping wing is much larger than the LEV on the rotating wing at the same Reynolds number, helping explain the peak in force observed at mid-downstroke in flapping wings. However, these observations do not help explain the different scaling of lift to power ratio between revolving and flapping wings – the LEV is reduced in size in low Reynolds number cases in both wing motion patterns and saturates in size for both at around Reynolds number = 800. Further examination of the results showed that the differences in lift to power ratio appeared because while the lift for the flapping wing decreases with decreasing Reynolds number, its power expenditure remains mostly unchanged whereas in the revolving wing, lift decreases while power expenditure increases (**Fig. 8a**). The simulations indicate that the drag force, which is responsible for most of the power expenditure, is dominated by viscous effects for the revolving wing and these effects grow with decreasing Reynolds number. In contrast, the drag on the flapping wing seems to be dominated by non-viscous added mass effects which are mostly independent of the Reynolds number. The relative independence of power expenditure on Reynolds numbers is the primary cause of the significantly higher efficiency of the lift generation of the flapping wing when compared to the revolving wing at low Reynolds number. The current study therefore clearly shows that at very small scales, hovering with flapping wings is intrinsically more advantageous than with revolving wings.

The current study of revolving vs. flapping wings is limited to a maximum Reynolds number of about 5000. This value was chosen since it is the operational Reynolds number for the hawkmoth

configurations have very comparable lift generation and power expenditure, would extend to higher Reynolds numbers. We note in closing that despite the similar performance of the two configurations at the higher Reynolds numbers, the underlying flow physics differ substantially, making extrapolation of these results from hovering flight to other situations such as forward flight or maneuvering, problematic. Further results of this study can be found in Zheng et al. (2013a).

C. Significance of Moment of Inertia in Insect Flight Maneuvers

In this study we examined the role that changes in body moment of inertia might play during flight maneuvers of insects. High-speed, high-resolution videogrammetry was used to quantify the trajectory and body conformation of Painted Lady butterflies (**Fig. 10**) during flight maneuvers; the 3D kinematics of the center of masses of the various body parts of the insect were determined experimentally. Measurements of the mass properties of the insect were used to parameterize a simple flight dynamics model of the butterfly. Even though the mass of the flapping wings is small compared to the total mass of the insect, these experiments and subsequent analysis reveal that changes in moment of inertia during flight are large enough to influence the maneuvers of these insects.



The established method for studying insect flight stability and maneuverability includes developing dynamic models that incorporate relevant details regarding mass properties, wing kinematics and aerodynamic forces; these models are then used to explore the stability and maneuverability of insects. In all of these studies however, the moment of inertia (MoI) of an insect is assumed to be constant in time.

Insect bodies consist of the head, thorax, abdomen and wings, and the assumption of time-invariant MoI for a flying insect is based on two underlying assumptions: the general assumption that the wings—which typically constitute a very small fraction of total body mass—do not contribute much to the MoI and the assumption that the head and body (thorax and abdomen) is a rigid entity that cannot change its shape or changes shape only slightly. With regard to the former, while it is certainly true that wings typically account for a very small fraction of the total body mass, they might account for a larger fraction of the MoI since the moment arm of the wings about the centre of mass (CoM) can be large. Indeed, the roll and yaw MoIs of larger flying animals such as birds and bats are dominated by wing inertia (Hedrick, 2011), which accounts for more than 90% of the total MoI of these animals. This, coupled with the flapping motion of the wings, could lead to non-negligible variations in MoI during flight. With regard to the latter notion – rigidity of the head, abdomen and thorax joints – insects such as butterflies and moths show notable articulation of their abdomen and thorax during flight and this could also result in a time-varying MoI. Indeed our measurements (**Fig. 11**) show significant variations in the MoI for the Painted Lady butterfly. The effect of these variations can be quantified by considering the conservation of angular momentum as given the equation below:

$$[I]\ddot{\theta} + [\dot{I}]\dot{\theta} = \tau \quad (\text{Eqn. 1})$$

where $[I]$ is the moment of inertia tensor, θ is the angular position and τ is torque. Typically only the effect of $[I]\ddot{\theta}$, the external aerodynamic torque is considered in explaining insect flight maneuvers. However, our experimental results suggest that both terms are of similar magnitude in the butterfly.

The estimated torque due to external aerodynamic forces and internal changes to moment of inertia during a butterfly pitch maneuver are shown in **Fig. 12**, with the variation in the external torque term shown as a band of possible values corresponding to the two extrema of pitch MoI. This plot shows that during this maneuver, the magnitudes of the torque component due to angular acceleration and the torque component due to the time rate of change of MoI are quite comparable. Thus, even though the wings of the Painted Lady butterfly only contribute about 7% of the total mass of the insect, the MoI changes induced by the movement of the wings likely affects the instantaneous dynamics of the insect during flight maneuvers. This effect therefore cannot be neglected without proper justification in insect flight dynamics studies. It remains to be studied if (and how) insects make use of this additional torque component during the many rapid, and oft-times complex, maneuvers that they exhibit in natural flight. Further results of this study can be found in Lin et al. (2013).

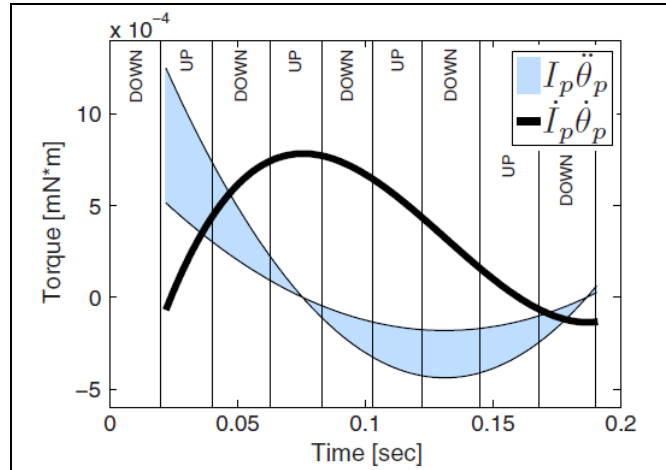
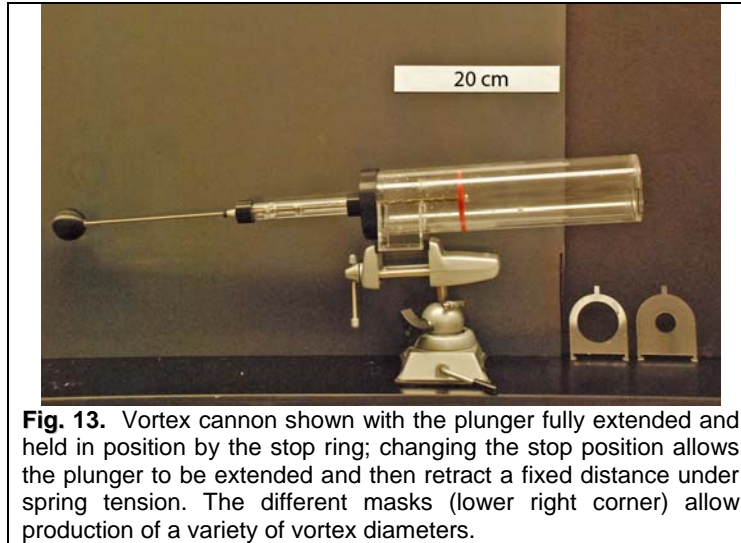


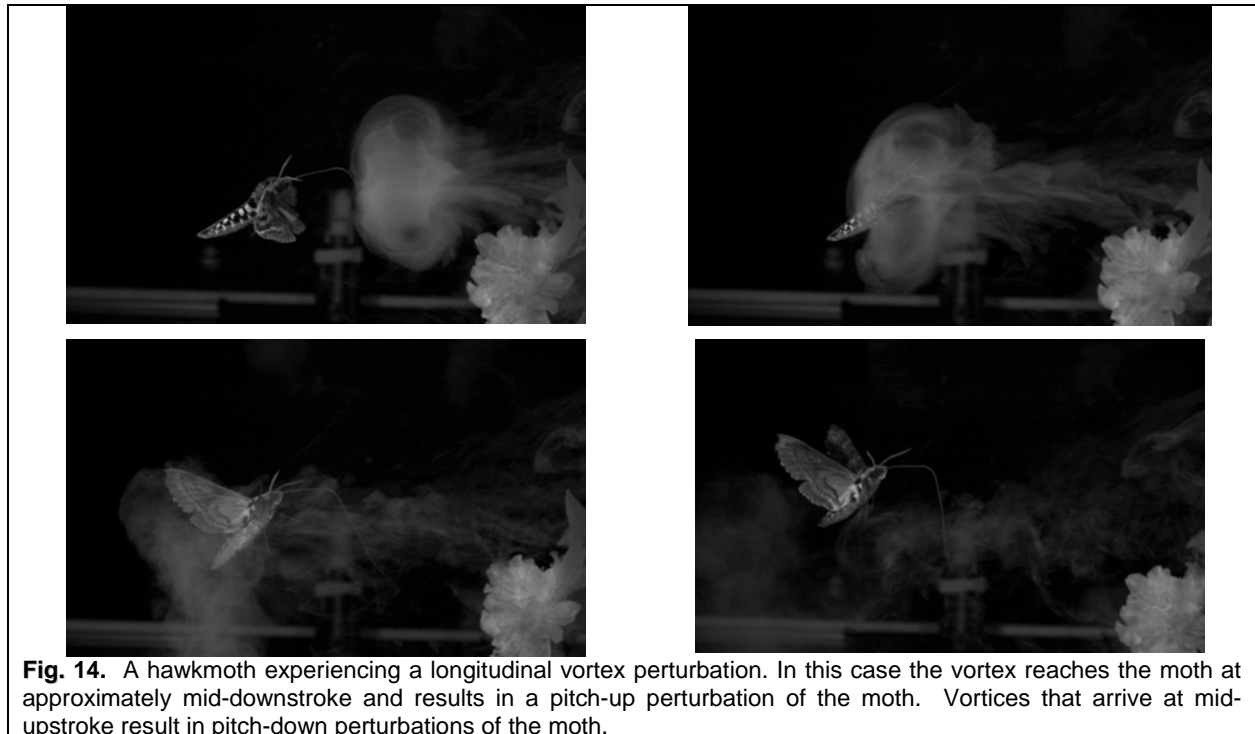
Figure 12. Components of rate of change of pitch angular momentum estimated using the upper and lower bounds of pitch MoI and the maximum time rate of change of MoI. Note that since the sign of \dot{I}_p changes within each flapping cycle, the effect of $\dot{I}_p \dot{\theta}_p$ may be positive or negative throughout the maneuver.

D. Experimental Assays of Moth Flight Perturbed by Vortex Rings

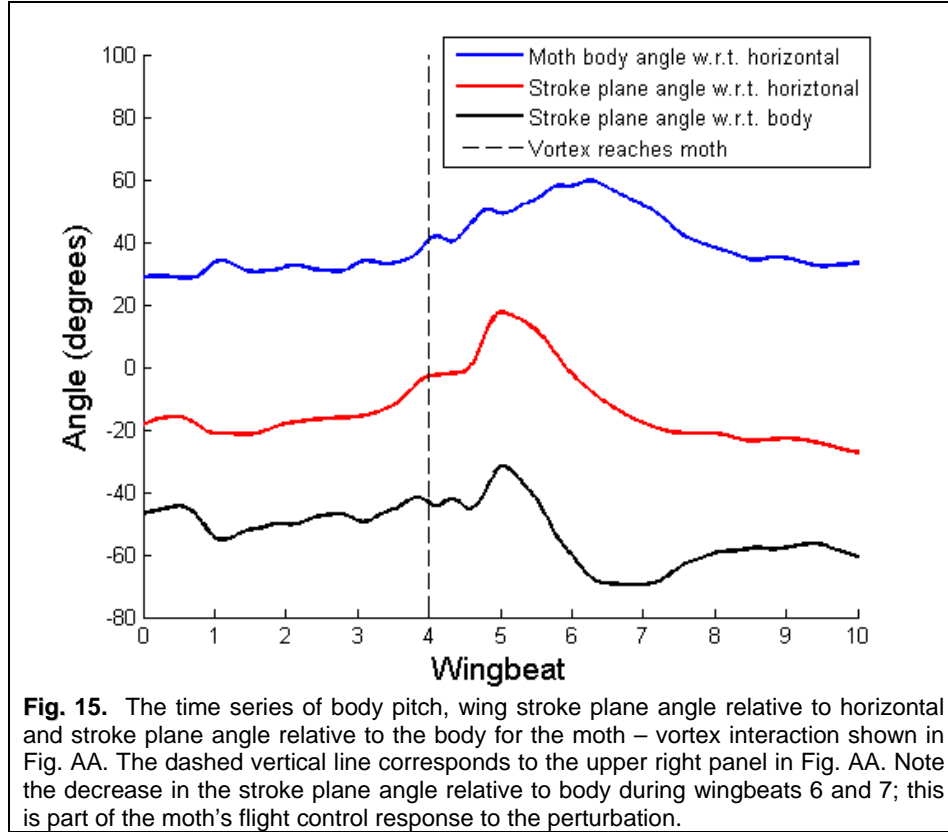
In pursuit of our objective of understanding how insects fly in the unsteady flows typical of urban environments, we developed an experimental technique for providing discrete flow perturbations to insects in hover via directed vortex rings. This effort was conducted in parallel with the computational and mathematical study of insect flight dynamics and stability in hover as described below in section E and a bio-inspired flight control strategy in Section F. The experimental results described below provide biological grounding for the CFD and mathematical modeling along with quantitative and qualitative results for comparison.



Vortex perturbation experiments were carried out in the moth flight chamber (**Fig. 3a**) using a spring-loaded plunger vortex gun with variable exit diameter and cylinder length (**Fig. 13**). Moth – vortex interactions produced large perturbations in the target moth (**Fig. 14**). Axial vortex perturbations like the one shown in the figure result in pitch perturbations; useful for studying flight stability in insects since longitudinal position and pitch orientation are typically identified as unstable in experimental or computational studies, e.g. Taylor and Thomas (2003) and Sun and Tang (2002) while lateral position and roll and yaw orientation are more stable Hedrick et al. (2009). The vortex perturbations were also found to produce different responses from the moth depending on the timing of the moth-vortex interaction. If the oncoming vortex reaches the moth during the downstroke, as in **Fig. 14**, the moth pitches up in response. If the vortex reaches the moth during the upstroke, the moth pitches down in response.

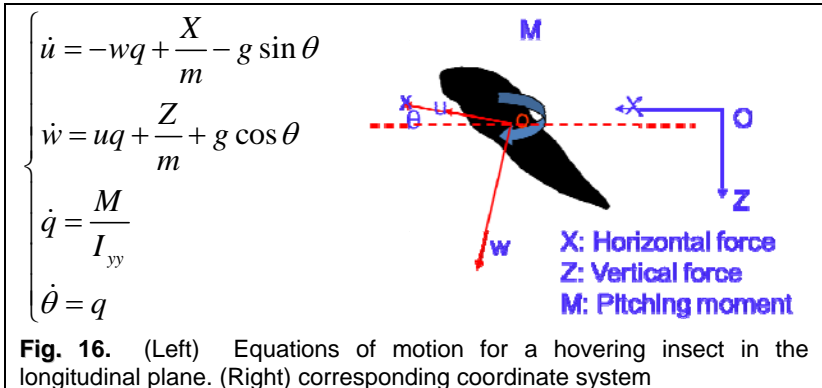


The principle wing motion response of the moth to these axial perturbations is to adjust the stroke plane angle of the wings with respect to the horizontal plane back toward the original, unperturbed position. **Figure 15** shows the complete time course of the moth's pitch perturbation in response to the vortex interaction from Figure AA along with the orientation of the wing stroke plane with respect to horizontal and also with respect to the moth's body axis. One wingbeat after the perturbation arrives, the moth begins changing its wing orientation with respect to the body, reaching a maximum deviation near wing stroke 6. The overall effect of changing the stroke plane angle so as to keep it close to the original orientation rather than allowing it to move along with the body is to provide a form of pendular stability in pitch as is explored in detail and implemented in the simulated moth in sections E and F below.



E. Flight Dynamics and Stability of an Insect in Hover

A key objective of the project was to understand how animals stabilize their flight in unsteady flows that are representative of urban environments. As a precursor to this, it was important to understand the intrinsic stability characteristics of a hovering insect. In the current study, we have focused our stability analysis on the hovering Hawkmoth (**Fig. 3**). Two different analyses have been conducted: the first is the so-called Linear Time Invariant (LTI) analysis which assumes a time-invariant base (equilibrium) state and the second is a Floquet stability analysis (FSA) which assumed a time-



periodic equilibrium state. FSA is more accurate for a large insect such as a Hawkmoth because the equilibrium state is indeed a limit cycle and the moment-of-inertia of the insect also varies periodically in time (see previous section). The stability analysis is restricted to the longitudinal plane in order to simplify the analysis. The basic equations of motion and the configuration are shown in **Fig. 16**.

The equations are linearized about the equilibrium conditions leading to a linear system for the perturbation of the form $\{\dot{x}\} = [A]\{x\}$, where $\{x\}^T = \{\delta u, \delta w, \delta q, \delta \theta\}$ is the perturbation vector. For the LTI and FSA models, the matrix $[A]$ is given by:

$$A = \begin{bmatrix} \frac{X_u}{m} & \frac{X_w}{m} & \frac{X_q}{m} & -g \\ \frac{Z_u}{m} & \frac{Z_w}{m} & \frac{Z_q}{m} & 0 \\ \frac{M_u}{I} & \frac{M_w}{I} & \frac{M_q}{I} & 0 \\ 0 & 0 & 1 & 0 \end{bmatrix} \quad \text{and} \quad A(t) = \begin{bmatrix} \frac{X_u(t)|_e}{m} & \frac{X_w(t)|_e}{m} - q_e(t) & \frac{X_q(t)|_e}{m} - w_e(t) & -g \cos \theta_e(t) \\ \frac{Z_u(t)|_e}{m} + q_e(t) & \frac{Z_w(t)|_e}{m} + u_e(t) & \frac{Z_q(t)|_e}{m} & -g \sin \theta_e(t) \\ \frac{M_u(t)|_e}{I(t)} & \frac{M_w(t)|_e}{I(t)} & \frac{M_q(t)|_e}{I(t)} & 0 \\ 0 & 0 & 1 & 0 \end{bmatrix}$$

respectively, where subscript ‘e’ refers to the equilibrium state. The X_u s etc. are the aerodynamic derivatives which are obtained by conducting Navier-Stokes simulations with corresponding imposed perturbation. Once the coefficients are obtained, the eigenvalues and eigenvectors of the above matrices are computed in order to determine the stability of the hovering insect. Both the analyses indicate that the hovering hawkmoth is marginally unstable in pitch and this observation is consistent with what is known about these and most other insects.

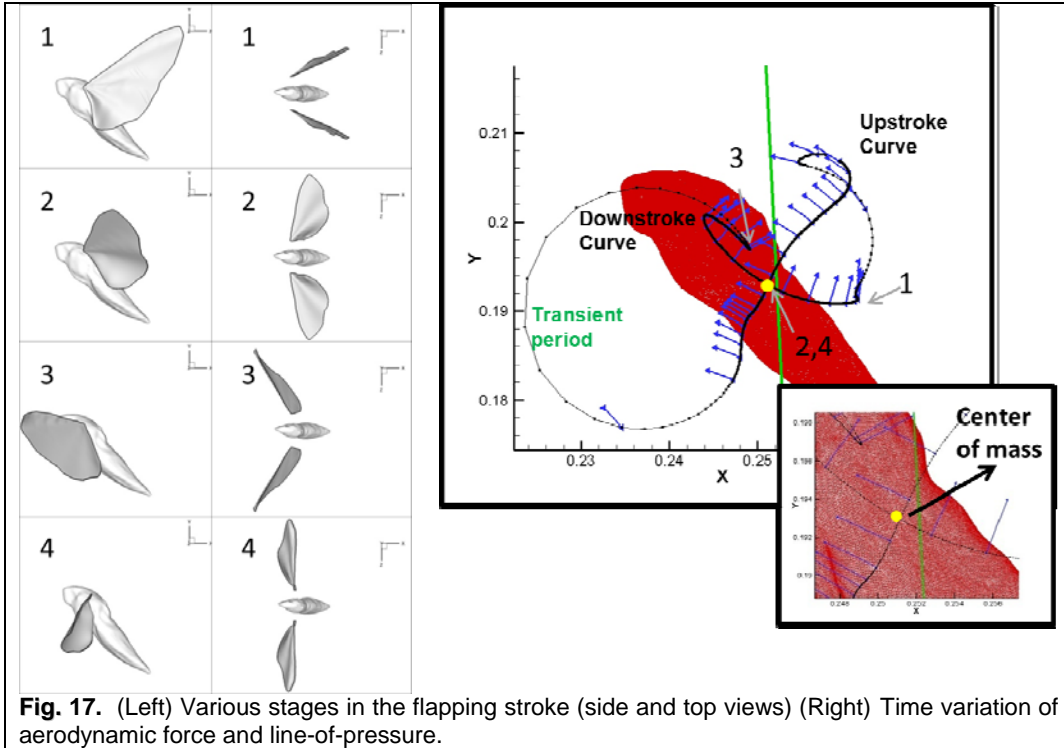


Fig. 17. (Left) Various stages in the flapping stroke (side and top views) (Right) Time variation of aerodynamic force and line-of-pressure.

The flow physics underlying this unstable behavior has been explored further. **Figure 17** shows the time-varying trajectory of the total-aerodynamic force generated by the wings along the instantaneous line-of-pressure (LOP). The vector shows the direction and magnitude of the force and the cross-product

of this force with the position vector relative to the center-of-mass indicates the pitching moment. The green line indicates the locus of points where placement of the center-of-mass (CoM) would generate a net zero change in the pitch of the insect over one cycle. The given CoM is slightly ahead of this line, and that is the cause for the pitch-up instability.

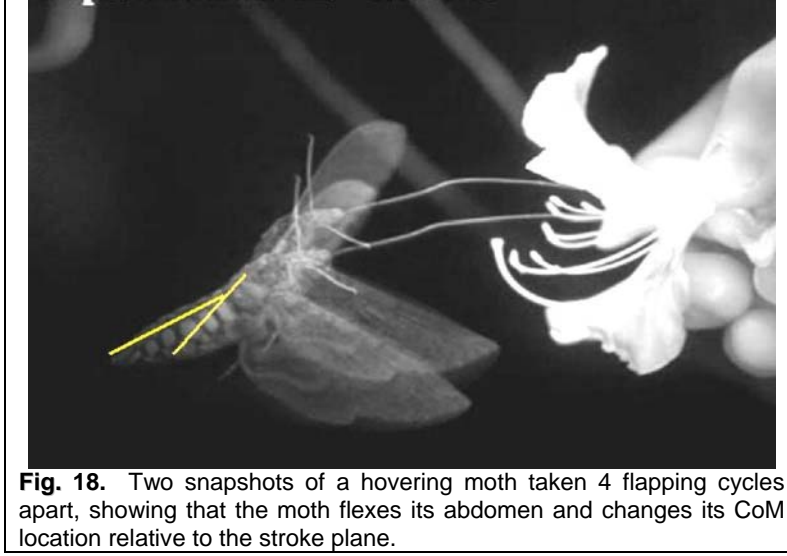


Fig. 18. Two snapshots of a hovering moth taken 4 flapping cycles apart, showing that the moth flexes its abdomen and changes its CoM location relative to the stroke plane.

F. Bioinspired Strategy for Flight Stabilization in Complex Aerodynamic Environments

The above analysis then suggests a possible strategy for active (feedback) stabilization; i.e. manipulation of the center-of-mass relative to the stroke-plane so that the mean location of the CoM is on the green line (Fig. 17). Examination of high-speed video data suggests that hawkmoth might indeed be doing exactly that to stabilize itself (see **Figs. 15 and 18**). Taking a cue from this, a strategy similar to this has been implemented in the current computational model of the insect. The CFD solver is coupled to a 3-degree-of-freedom flight dynamics model of the insect and we also include a flight controller that adjusts the relative angle between the body and the stroke plane at every time-step so as to keep it the same as the unperturbed case.

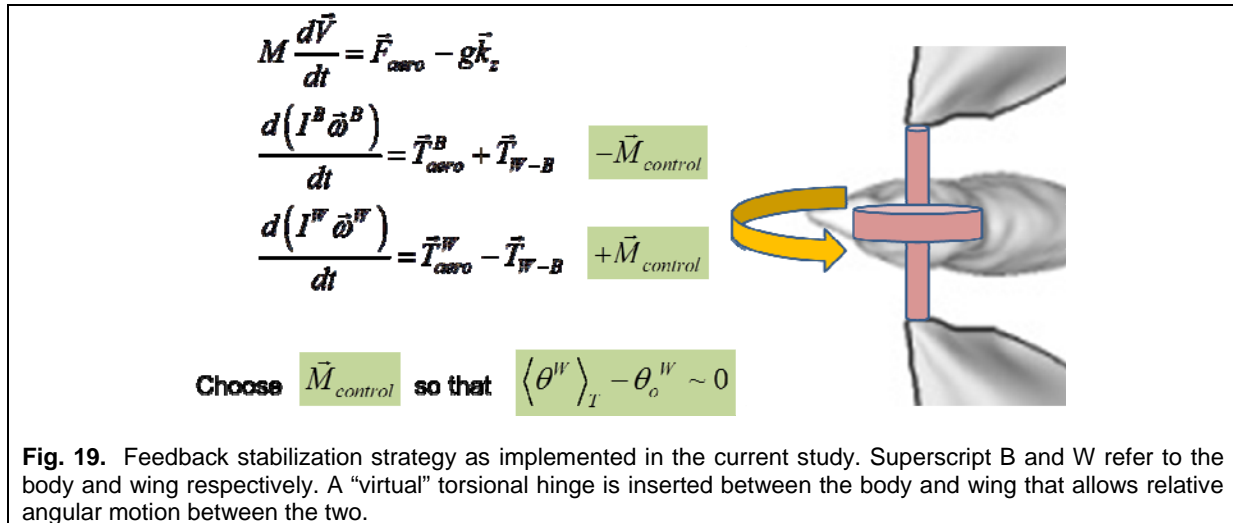
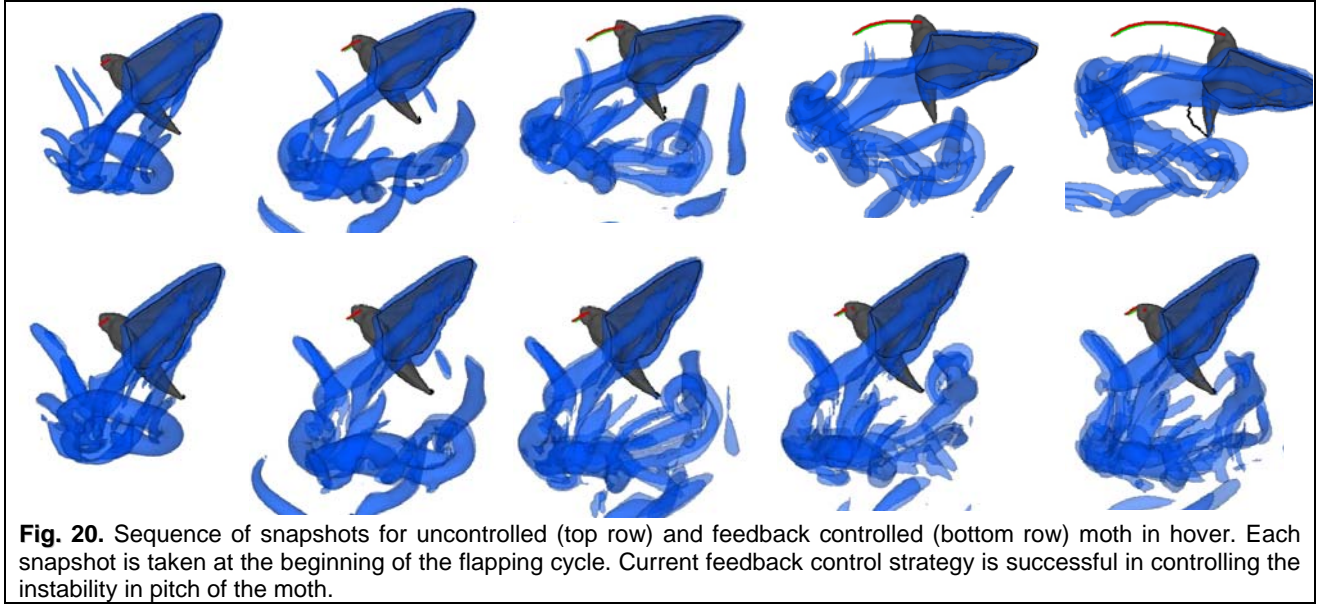
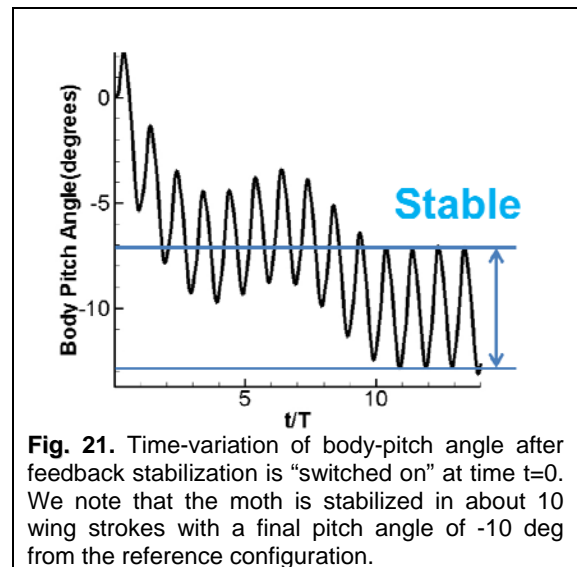


Figure 19 shows the mathematical formulation and the notional view of the feedback flight control strategy that has been implemented. We separate the dynamical equations of the wing and body and insert a “virtual” controllable torsional hinge between the body and wing. A moment M_{control} can now be applied at the hinge in order to change the relative angle between the wing stroke plane and the body. The current strategy is to use this to reduce the excursion of the stroke plane from the nominal value; i.e. $\langle \theta^w \rangle_T \rightarrow \theta_0^w$.



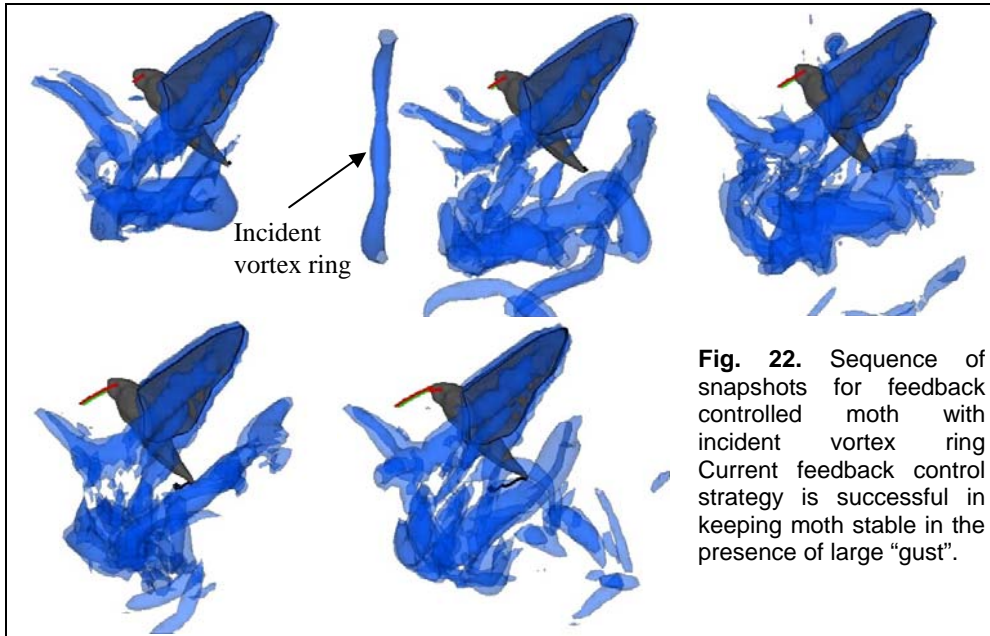
The above feedback flight control strategy was first applied to stabilization of moth flight in quiescent flow. As indicated by the earlier stability analysis, moths are open-loop unstable in hover and the intention here was to assess the effectiveness of the above strategy to produce a stable hover in the virtual moth. **Figure 20** shows snapshots of the moth with and without the active stabilization strategy implemented and we can clearly see the rapid pitch-up instability of the moth without control. On the other hand, the current feedback flight control strategy is successful in stabilizing the hover. **Figure 21** shows that it takes about 10 flapping cycles for the moth to reach an equilibrium, and the final orientation of the moth is approximately 10 deg. different from the starting configuration.

Given the ultimate objective of the current project was to understand the stabilization of insects in gusty/unsteady flows, we proceeded to examine the effectiveness of the feedback flight control strategy in a perturbed flow. The perturbation was provided by impinging vortex rings which matched the experiments (see Sec. D). We note that the strength of the vortex rings is such that it produces velocity perturbations that are 50-80% of the wing-tip velocity. Thus, by any measure, these perturbations are to be considered “large”. It is therefore not clear at the outset if the flight control strategy that works for infinitesimal perturbation will work for large perturbations. Furthermore, the vortex ring impinges on the insect from the anterior in such a way such as to impart a pitch-up impulse. Thus, this is a highly destabilizing perturbation for the



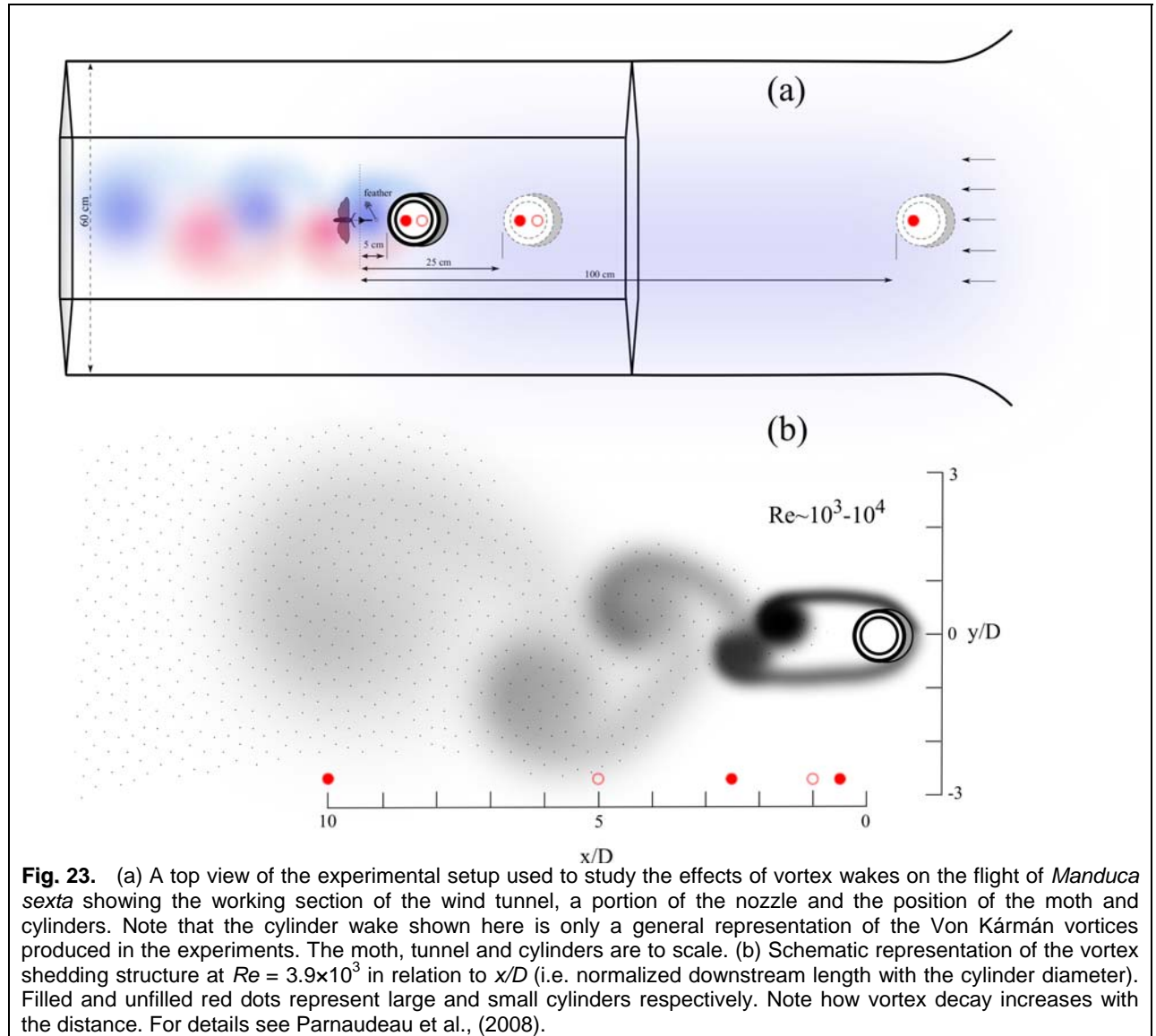
moth and provides a very strong test for the stabilization strategy. **Figure 22** shows the results for this large-perturbation case and they clearly demonstrate that the strategy is successful in stabilizing the insect even for a massive perturbation. While there is a large translational excursion in the location of the moth due to the net momentum transferred to the moth by the vortex ring, the moth maintains a stable orientation during the vortex encounter.

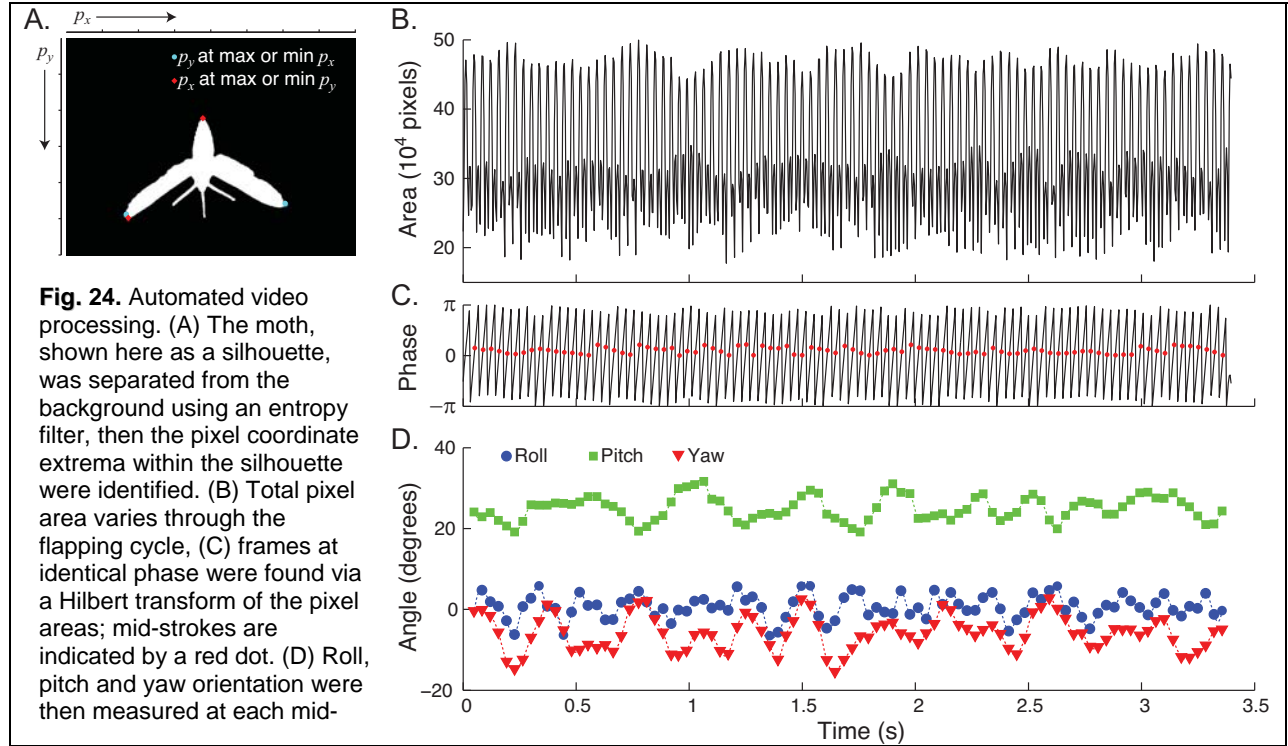
Work continues on completing this component of the project and we expect to prepare a journal publication on this in the coming year.



G. Analysis of a Flying Insect in Perturbed Flows

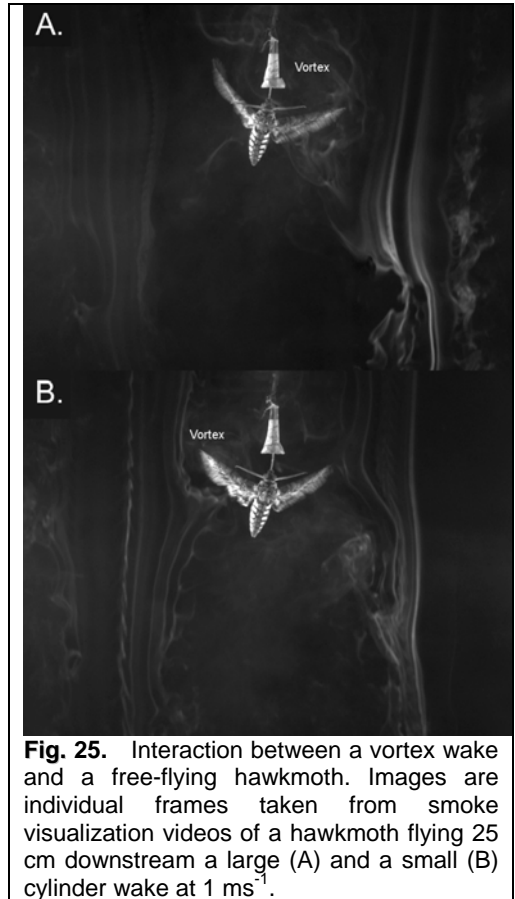
Shedding of vortices is a common phenomenon in the lower atmosphere over a wide range of spatial and temporal scales (Ogawa, 1993), particularly in urban “city canyon” environments central to the objectives of this research effort (**Fig. 1**). However, it is unclear how these vortices of varying temporal and spatial scales affect the flight performance of flying animals. In order to investigate these interactions we trained seven hawkmoths (*Manduca sexta*) (wingspan ~9 cm) to fly and feed in a wind tunnel under steady flow (controls) and in the Von Kármán vortex street of vertically oriented cylinders (two different cylinders with diameters of $x=10$ and $x=5$ cm) at speeds of 0.5, 1 and 2 ms^{-1} (**Fig. 23**). Cylinders were placed at distances of $D=5$, $D=25$ and $D=100$ cm upstream of the moths, resulting in non-dimensional cylinder placements (x/D) of 0.25, 2.5 and 10 for the large cylinder and 0.5, 5 and 20 for the small cylinder. Due to decay of the vortex with distance, we found that the moth was wholly unperturbed by the small cylinder placed 100cm upstream and this case was not considered further. The response of the moths to these perturbed flows were quantified via multi-camera high speed videography. A total of 7,421 flapping cycles were analyzed from the high speed video recordings using a set of automated moth identification routines developed for this project (**Fig. 24**).



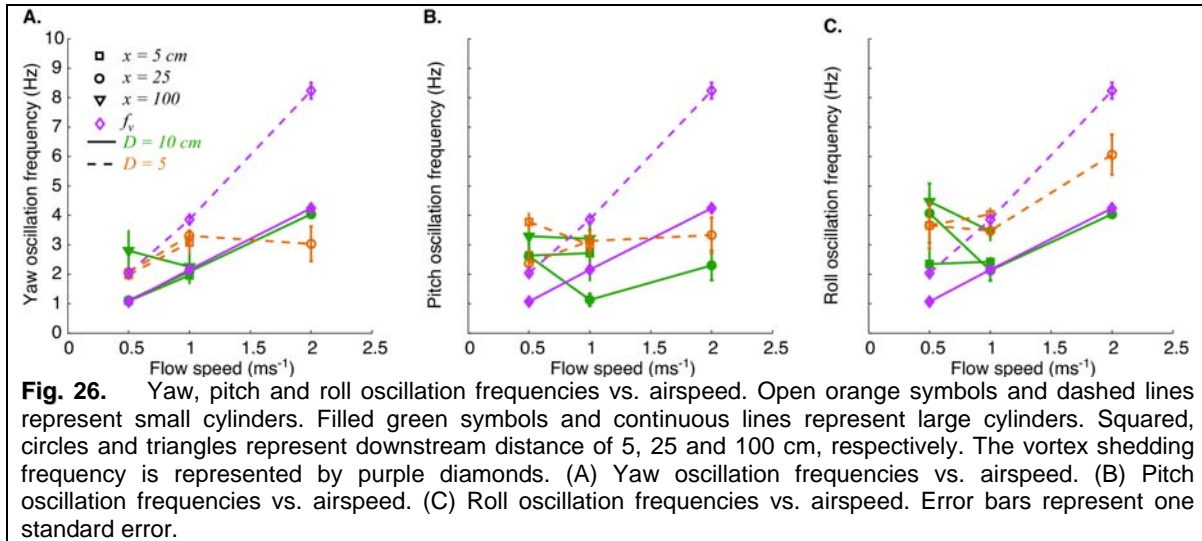


Moths regularly interacted with the Von Kármán vortex street (**Fig. 25**) and exhibited large amplitude yaw oscillations coupled with modest oscillations in roll and pitch (**Fig. 26**), and slight increases in wingbeat frequency when flying in both the near (recirculating) and middle (vortex dominated) wake regions. Wing flapping amplitude did not vary among treatments. Yaw and roll oscillations were synchronized with the vortex shedding frequencies in moths flying in the wake of the large cylinder at all speeds. In contrast, yaw was not synchronized with the shedding frequency of small vortices at speeds above 1 ms^{-1} . Oscillations in body orientation were also substantially smaller in the small cylinder treatment when compared to the large cylinder, regardless of temporal or non-dimensional spatial scale. These results show that the moth response depends on the dimensional rather than non-dimensional vortex scale. In general, flight disruptions produced by the cylinder wakes were qualitatively similar among the recirculating and vortex dominated wake regions; the magnitude of disruptions, however, declined gradually with downstream distance. At $x/D = 10$ those effects practically disappeared. Similarly, vortices smaller than a wingspan produced roll and yaw perturbations that were synchronized with vortex shedding at all speeds, except for yaw at 2 ms^{-1} ; these perturbations, however, were smaller than those elicited by the large cylinder at all air speeds and downstream distances.

The qualitative similarity of flight disruptions observed in hawkmoths flying in different wake regions was unexpected. We initially hypothesized that the dominant retrograde streamwise flow in the



near wake region ($x/D < 2$) would produce pitch oscillations while locations further downstream where cross-stream flow fluctuations are stronger would produce roll or yaw oscillations. Instead, all perturbation inputs produced similar outputs, suggesting that the moth's dynamic stability and control properties play a large role in determining the outcome of these below wingbeat frequency events. For example, pitch may be controlled on a short timescale by the moth since it is found to be unstable in most control analyses of flapping flight and is also heavily involved in fore-aft maneuvers in hawkmoths. In contrast, yaw and roll may receive less control input (and thus may vary more widely) since both are damped in flapping flight. Further results of this study can be found in Ortega-Jimenez et al. (2013).



H. Publications Resulting From Grant

1. Victor Manuel Ortega-Jiménez, Jeremy S.M. Greeter, Mittal, R and Hedrick, T. "Hawkmoth Flight Stability in Turbulent Vortex Streets" in review, *Journal of Experimental Biology*.
2. L. Zheng, T. L. Hedrick, R. Mittal, "A comparative study of the hovering efficiency of flapping and revolving wings", *Bioinspiration and Biomimetics*, Vol. 8 (3), pp:036001-13, 2013.
3. L. Zheng, T. L. Hedrick, R. Mittal, "A multi-fidelity modelling approach for evaluation and optimization of wing stroke aerodynamics in flapping flight", *Journal of Fluid Mechanics*, Vol. 721, pp:118-154, 2013.
4. L. Zheng, T. L. Hedrick, R. Mittal, "Time-varying wing-twist improves aerodynamic efficiency of forward flight in butterflies", *PLoS ONE*, Vol. 8(1), e53060, 2013.
5. T. Lin, R. Mittal, L. Zheng and T. Hedrick, "The significance of moment-of-inertia variation in flight manoeuvres of butterflies", *Bioinspiration and Biomimetics*, 7 044002 doi:10.1088/1748-3182/7/4/044002.
6. L. Zheng, Rajat Mittal and Tyson L. Hedrick, "A Search for Optimal Wing Strokes in Flapping Flight: Can Engineers Improve Upon Nature?" 28th Applied Aerodynamics Conference, Chicago, IL, AIAA 2010-4944, 28 June – 1 July.

I. Theses/Dissertations Associated with Grant

1. An Integrated Numerical-Experimental Study of the Aerodynamics of Flapping Flight in Insects, Lingxiao Zheng , PhD Dissertation, August 2012, Mechanical Engineering, Johns Hopkins University.

J. Honors & Awards Received

- Tiras Lin (Undergraduate Student, JHU): 2013 Churchill Fellowship.
- Rajat Mittal (PI) joined the editorial board of the *Journal of Experimental Biology*. (2013).
- Tyson Hedrick (Co-PI) received a NSF CAREER award in 2013.
- Tyson Hedrick (Co-PI) joined the editorial board of the *Journal of Theoretical Biology*. (2013).
- Jeremy Greeter (Graduate Student, UNC Chapel Hill) received a National Defense Science and Engineering Graduate Fellowship (2012)
- Chao Zhang (Graduate Student, JHU): 3rd Place at the 2012 AIAA Region I Young Professional, Student, and Education Conference for his presentation titled “Flight Stabilization with Flapping Wings in Gusty Environments.”
- Rajat Mittal (PI) joined the editorial board of the *Frontiers of Computational Physiology and Medicine*. (2011).
- Rajat Mittal elected to Fellowship in the American Society of Mechanical Engineers (2011).
- Rajat Mittal elected to Fellowship in the American Physical Society (2011).
- Tiras Lin (Undergraduate Student, JHU): 2nd Place at the 2011 AIAA Region I Young Professional, Student, and Education Conference for his presentation titled “Understanding the Role of Moment-of-Inertia Variation in Insect Flight Maneuvers.”
- Tiras Lin (Undergraduate Student, JHU): 3rd Place at the 2010 AIAA Region I Young Professional, Student, and Education Conference for his presentation titled “Study of Insect Flight Dynamics Using High-Speed Videogrammetry”.

K. Personnel Supported

- | | |
|----------------------------|---|
| • Lingxiao Zheng | Doctoral Student, Johns Hopkins University |
| • Chao Zhang | Doctoral Student, Johns Hopkins University |
| • Tiras Lin | Undergraduate student, Johns Hopkins University |
| • Rajat Mittal | Professor, Johns Hopkins University |
| • Tyson Hedrick | Assoc. Professor, UNC at Chapel Hill |
| • Victor M. Ortega-Jiménez | Postdoctoral Researcher, UNC at Chapel Hill |
| • Jeremy Greeter | Doctoral Student, UNC at Chapel Hill |

Bibliography

1. Aono, H, W. Shyy, and H. Liu, (2009) Near wake vortex dynamics of a hovering hawkmoth," *Acta Mechanica Sinica*, vol. 25, pp. 23-36.
2. Balachandar, S. Mittal R. and Najjar F.M. (1997). Properties of the Mean Recirculation Region in the Wakes of Two Dimensional Bluff Bodies, *J. Fluid Mech.* vol. 351, 161-201.
3. Casey, T. M. 1976 Flight energetics of sphinx moths: power input during hovering flight. *The Journal of Experimental Biology* vol. 64, 529-543.
4. Ellington C P, Van Den Berg C, Willmott A P and Thomas A L R 1996 Leading-edge vortices in insect flight *Nature* vol. 384 626–30
5. Hedrick, T. L. (2011). Damping in flapping flight and its implications for manoeuvring, scaling and evolution. *The Journal of Experimental Biology* vol. 214, 4073-4081.
6. Hedrick, T. L., Cheng, B. and Deng, X. (2009). Wingbeat Time and the Scaling of Passive Rotational Damping in Flapping Flight. *Science* vol. 324, 252-255.
7. Lin, T. Mittal, R., L. Zheng and T. Hedrick, (2012) "The significance of moment-of-inertia variation in flight manoeuvres of butterflies", *Bioinspiration and Biomimetics*, 7 044002 doi:10.1088/1748-3182/7/4/044002.
8. Liu H and Kawachi K 2001 Leading-edge vortices of flapping and rotary wings at low Reynolds number Fixed and Flapping Wing Aerodynamics for Micro Air Vehicle Application ed T J Mueller (American Institute of Aeronautics and Astronautics) pp 275–85
9. Mittal R, and G. Iaccarino, (2005) Immersed boundary methods," *Annual Review of Fluid Mechanics*, vol. 37, pp. 239-261, 2005.
10. Mittal, R, H. Dong, M. Bozkurtas, F. M. Najjar, A. Vargas, and A. V. Loebbecke, (2008) A versatile sharp interface immersed boundary method for incompressible flows with complex boundaries," *Journal of Computational Physics*, vol. 227, pp. 4825-4852, 2008.
11. Ogawa, A. (1993). Vortex Flow. CRC Press, New York, NY.
12. Ortega-Jiménez, V.M. Jeremy S.M. Greeter, Mittal, R and Hedrick, T. (2013) "Hawkmoth Flight Stability in Turbulent Vortex Streets" in review, *Journal of Experimental Biology*.
13. Parnaudeau, P., Carlier, J., Heitz, D. and Lamballais, E. (2008). Experimental and numerical studies of the flow over a circular cylinder at Reynolds number 3900. *Phys. Fluids* 20, 085101
14. Prasad, A. and Williamson, C. H. K., (1996) "The Instability of the Separated Shear Layer from a Bluff Body," *Phys. Fluids*, vol. 8, no. 6, pp. 1347-1349.
15. Roshko, A. (1954) "On the Development of Turbulent Wakes from Vortex Streets," NACA Report 1191.
16. Seo J. H. and Mittal, R. "A sharp interface immersed boundary method with improved mass conservation and reduced spurious pressure oscillations", *Journal of Computational Physics*, 2011, vol. 230, Issue 19, pp. 7347-7363.
17. Sun, M. and Tang, J. (2002). Unsteady aerodynamic force generation by a model fruit fly wing in flapping motion. *The Journal of Experimental Biology* vol. 205, 55-70.
18. Stevenson, R. D. & Josephson, R. K. 1990 Effects of operating frequency and temperature on mechanical power output from moth flight muscle. *The Journal of Experimental Biology* vol. 149, 61-78.
19. Taylor, G. K. and Thomas, A. L. R. (2003). Dynamic flight stability in the desert locust *Schistocerca gregaria*. *The Journal of Experimental Biology* vol. 206, 2803-2829.

20. Zheng, L., Hedrick, T., Mittal, R., (2013a) “A comparative study of the hovering efficiency of flapping and revolving wings”, *Bioinspiration and Biomimetics*, vol. 8 (3), pp:036001-13, 2013.
21. Zheng, L., Hedrick, T. L. Mittal, R., (2013b) “A multi-fidelity modelling approach for evaluation and optimization of wing stroke aerodynamics in flapping flight”, *Journal of Fluid Mechanics*, vol. 721, pp:118-154, 2013.